THE JOURNAL OF PHYSICAL CHEMISTRY C

Article

pubs.acs.org/JPCC

Modeling the Water Splitting Activity of a TiO_2 Rutile Nanoparticle

Enrico Berardo and Martijn A. Zwijnenburg*

Department of Chemistry, University College London, 20 Gordon Street, London, WC1H 0AJ, U.K.

Supporting Information

ABSTRACT: We explore, from a theoretical perspective, the effect of particle size on the photocatalytic water splitting activity of TiO_2 rutile (nano)particles by a combination of explicit quantum chemistry calculations on a hydroxylated rutile nanoparticle in a realistic solvation environment and a comparison with the calculated properties of bulk rutile (surfaces) from the literature. Specifically, we use density functional theory (DFT) and time-dependent DFT to calculate the nanoparticle thermodynamic driving force for the water splitting half-reactions and identify in the process the crucial role of self-trapping of the free charge carriers responsible for proton reduction and water oxidation.

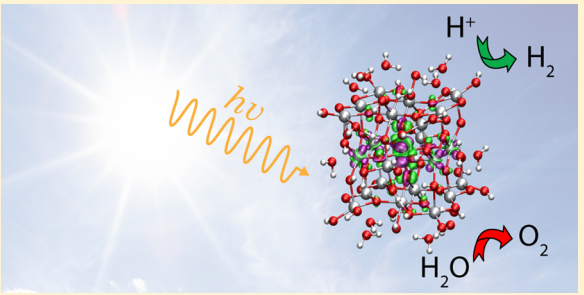

INTRODUCTION

TiO_2 nanoparticles are the quintessential photocatalyst, a material that allows a reaction to happen in the presence of light that otherwise would not take place. Loaded with a noble metal cocatalyst (Pd, Pt, Rh), both rutile[1−4] and anatase[5−7] nanoparticles catalyze the overall splitting of water into molecular hydrogen and oxygen when illuminated with ultraviolet light, while without noble metals they act as photocatalysts for the degradation of organic molecules[8−11] and drive the individual water splitting half-reactions in the presence of a suitable electron or hole donor.[12−14] Some of these reactions are endothermic, and part of the photon energy becomes incorporated in the reaction products (e.g., overall water splitting), a situation commonly referred to as artificial photosynthesis or solar fuel synthesis.[15] In other cases, the photocatalyzed reactions are exothermic in the dark, e.g., organic pollutant degradation, and the illuminated photocatalyst acts as a catalyst in the classical chemical sense and improves the reaction rate.

Even if only active in the ultraviolet part of the solar spectrum, at least in the absence of heavy doping, TiO_2 nanoparticles and related nanostructures, e.g., thin films, are probably the world's most studied photocatalyst. TiO_2 is hence the natural starting point for computational studies into the fundamental physical and chemical processes that underlie photocatalysis in inorganic solids, work that is needed because, even in the case of TiO_2, many fundamental issues are still unresolved. For example, there is an ongoing discussion about the relative position of the (reduction potentials associated with the) conduction band in anatase and rutile,[16−20] as well as the defect chemistry of TiO_2 and how this can be used to reduce the optical gap from the ultraviolet to the visible part of the spectrum.[19] Finally, there is the issue of the dependence of the photocalytic activity on particle size and morphology, about which there are very contrasting reports in the literature. For example, work on the reduction of protons, as part of overall water splitting or in the presence of a sacrificial electron donor, suggests a decrease in photocatalytic activity with decreasing particle size,[7,21,22] while other studies that focus on the degradation of organic molecules report an increase in activity instead.[3,13,23,24]

During use as a photocatalyst, the particle can exist in a number of different electronic states: the electronic ground state (P), an electronically excited excitonic state (P*), or indeed an anionic (P^-) or cationic (P^+) state. Starting from the ground state, absorption of light with energy higher than the optical gap results in the excitation of the particle and the formation of an exciton, an excited electron−hole pair bound through their mutual electrostatic interaction. This exciton subsequently can dissociate into a free electron and free hole, where free signifies that the excited electron and hole are sufficiently spatially separated so that their effective interaction is negligible, for example, by being localized on different particles. This free electron and hole can take part in interesting chemistry but also recombine to re-form an exciton in a process referred to as electron−hole recombination. Excitons can decay at any stage back to the ground state under the emission of light, (photo)luminescence, or via a nonradiative route, internal conversion, where the excess energy is dissipated in the form of phonons (vibrations).

Both the exciton and the free charge carriers can in principle localize on a fragment of the particle (self-trap, e.g., a self-trapped exciton) or become trapped on a structural defect (e.g., a free electron trapped by an oxygen vacancy).[25−29] Especially, self-trapped exciton formation appears to be very structure sensitive; bulk rutile only has free nontrapped excitons, while in bulk anatase, excitons appear to self-trap.[30−33] Experimentally, self-trapping is observable by the different spectroscopic

Received: February 13, 2015
Revised: May 20, 2015
Published: May 21, 2015

DOI: 10.1021/acs.jpcc.5b01512
J. Phys. Chem. C 2015, 119, 13384−13393

signatures of free and trapped states. For example, in the case of excitons, a red shift between the optical gap and the photoluminescence maxima is a signature of a self-trapped exciton.

Modeling such complex processes is not straightforward, especially deciding what to include and what not. However, we believe a number of essential features should be incorporated in the model. Both the free charge carriers (Figure 1A) and the exciton (Figure 1B) can in principle drive the water splitting half-reactions by providing electrons and holes with the necessary chemical potential. Any attempt at modeling a photocatalyst should therefore, in our opinion, consider both free charge carriers and excitons. This is especially true when considering nanoparticles. For many bulk solids the difference between the energy required for creating a pair of free charge carriers and that needed to make an exciton is very small (for example, 4 meV for bulk rutile[34]) and the potentials associated with excitons and free charge carriers thus approximately degenerate. The same is not necessarily true in the case of nanoparticles, and excitons in such systems might be hard(er) to dissociate. Furthermore, because of the known potential for (self)trapping in TiO_2 (see above), one ideally should also consider the effect of structural relaxation when studying photocatalysts. Finally, taking into account the need to understand the explicit effect of particle size and the fact that at least in the case of overall water splitting, the photocatalyst will operate immersed in water, it appears sensible to explicitly study hydroxylated nanoparticles, the surface of which is further covered by a monolayer of adsorbed water molecules. The latter explicit description of surface water is possibly used in conjunction with a dielectric continuum solvation model to reproduce the effect of bulk water. Relevant previous work on TiO_2 generally did not consider excitons and focused instead on studies of free charge carriers either in periodic 2D slabs[26,28,35] or in nanoparticles,[19,36−39] while the selected papers[40−55] that do consider excitons, mostly in the case of nanoparticles, as a rule do not take into account exciton self-trapping and often focus on unhydroxylated naked particles in vacuum.

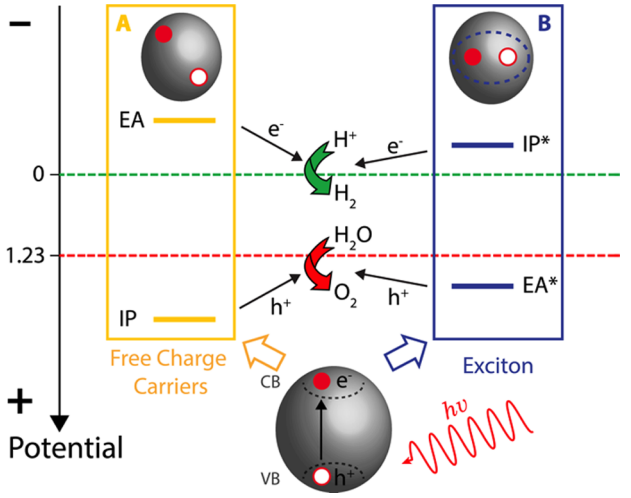

Figure 1. Scheme showing how the (standard) reduction potentials (IP, EA, EA*, and IP*) of the ideal photocatalyst (nanoparticle) straddle the proton reduction and water oxidation potentials (green and red broken lines for HER and OER, respectively). $h\nu$ defines the energy of the photon absorbed by the nanoparticle. e^- and h^+ stand for electron and hole, respectively, while VB and CB are the valence and conduction bands of the particle. Box A represents the free charge carriers scenario, where the excited electron and hole are spatially separated within the particle and have negligible Coulombic interaction. Box B represents the exciton scenario, where the excited electron and hole are strongly interacting and can be described as an excited electron−hole pair, or exciton.

Following the logic set out above, we report here our first results of DFT/TD-DFT calculations on a ∼1 nm hydroxylated rutile nanoparticle (taken from previous work by Freisner and co-workers;[36,38,39] see Figure 2), where we explicitly include the effect of solvation and trapping. This nanoparticle structure, even if small compared to rutile nanoparticles synthesized experimentally, is perhaps the smallest rutile particle that still preserves essential features of the bulk structure.

We report a range of optical and excited state properties for this particle including the optical gap, the predicted photoluminescence signal, the sites within the particle on which the exciton self-traps, and the structural distortion associated with the localization. We also calculate the standard reduction potentials of the free charge carriers and exciton in this particle and compare them with those of the water splitting half-reactions to examine the thermodynamic ability of this rutile particle, and small TiO_2 nanoparticles in general, to drive the photocatalytic splitting of water. Finally, we use all these data to discuss how the photocatalytic ability of nanoparticles might differ from their larger counterparts and the role of surface flexibility therein.

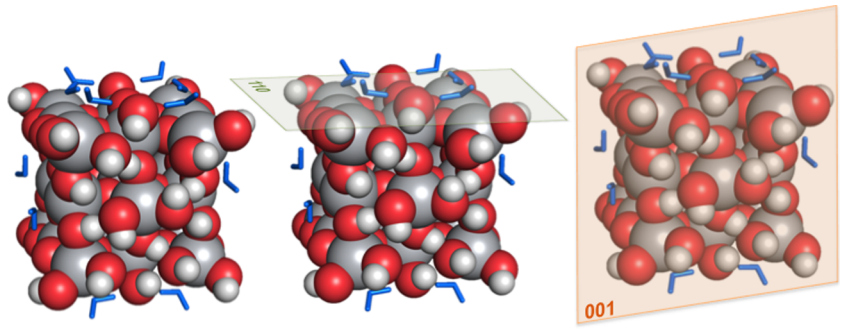

Figure 2. TiO_2 rutile nanoparticle containing 23 TiO_2 units and 34 water molecules, 18 split as hydroxyl groups on the particle's surface and 16 in their molecular state (pictured as blue lines), which amounts to a total of 171 atoms. The crystal planes that define the particle are also shown: four 110 (light green, top middle figure) and two 001 planes (light orange, top right figure). Red spheres denote oxygen atoms, whereas gray and white spheres represent titanium and hydrogen atoms, respectively.

DOI: 10.1021/acs.jpcc.5b01512
J. Phys. Chem. C 2015, 119, 13384−13393

THEORETICAL PICTURE

In the following section we will discuss a possible theoretical picture of photocatalysis, from the perspective of the reaction that is photocatalyzed and that of the photocatalyst. In the latter we will build on our recent work on photocatalytic polymers.[56−58]

Water Splitting Reaction Perspective. The overall water splitting reaction is a combination of two half-reactions (both expressed as reductions, in line with convention):

$$2H^+ + 2e^- \rightleftarrows H_2 \quad (A)$$

$$O_2 + 4H^+ + 4e^- \rightleftarrows H_2O \quad (B)$$

During water splitting half-reaction A, the hydrogen evolution reaction (HER) will run in the forward direction, the reduction of protons to molecular hydrogen, and in reaction B, the oxygen evolution reaction (OER) will run in the direction opposite to that written, oxidation of water to molecular oxygen and protons.

In order for both of these half-reactions to take place and overall water splitting to occur, a photocatalyst will have to provide electrons for the HER and accept electrons, or in other words donate holes, to drive the OER. The (standard) reduction potential of the electrons and holes provided by a photocatalyst should thus straddle those of HER and OER half-reactions (see Figure 1A and Figure 1B). Moreover, as the HER experimentally has a standard reduction potential of 0 V relative to the standard hydrogen electrode (SHE) at pH 0 and the OER a standard reduction potential of 1.23 V, a successful photocatalyst needs therefore to provide at least this amount of potential to split water. In practice, a larger overall potential than 1.23 V (e.g., 1.8 V) is required to overcome energetic losses and kinetic barriers, the difference between the effective and equilibrium potentials being the overpotential. For endergonic overall redox reactions other than water splitting, e.g., reduction of protons in the presence of a sacrificial electron donor, a very similar analysis can be performed.

In the case of overall redox reactions that are exergonic in the dark, the situation is slightly different. As there is no need for the photocatalyst to drive such reactions to make them thermodynamically feasible, the photocatalytic activity arises purely because the photocatalysts allow for larger overpotentials to be overcome than possible in its absence. We plan to discus the case of endergonic reactions in future work and focus here exclusively on the case of photosynthesis.

Photocatalyst Perspective. As discussed in the Introduction, a photocatalyst can provide electrons and holes to drive redox reactions in the form of free charge carriers (Figure 1A) and (as part of) excitons (Figure 1B). When analyzing the ability of a particle (P) to act as a photocatalyst for the redox reactions discussed above, we thus, following our previous work,[56,57] need to consider the potentials associated with four different half-reactions (written, again in line with convention, as reductions):

$$P^+ + e^- \rightleftarrows P^* \quad (C)$$

$$P^* + e^- \rightleftarrows P^- \quad (D)$$

$$P + e^- \rightleftarrows P^- \quad (E)$$

$$P^+ + e^- \rightleftarrows P \quad (F)$$

where in half-reactions C and E, the exciton and the free electron, respectively, serve as reductants for species in solution; the particle donates electrons, and the half-reactions will run in the opposite direction to that written above. In the other two half-reactions (D and F), the particle accepts electrons (donates holes) and the exciton and the free holes act as oxidants for species in solution. The reduction potential of half-reaction F is equal to the ionization potential, the free energy required to remove an electron from the top of the photocatalyst's valence band, and is hence further labeled as IP. Similarly, the reduction potential of half-reaction E equals the electron affinity, the free energy released upon adding one electron to the bottom of the photocatalyst conduction band, and labeled as EA. Finally, the potentials of half-reactions C and D can be thought of as the excited state ionization potential IP*, the free energy required to remove the excited electron from the exciton, and the excited state electron affinity EA*, the free energy released upon adding an electron to the exciton and annihilating the exciton's hole component, respectively.

The thermodynamic preference for excitons versus free charge carriers can be analyzed in terms of the following nonredox reaction:

$$P^* + P \rightleftarrows P^+ + P^- \quad (G)$$

The (free) energy change associated with reaction G is commonly referred to as the exciton binding energy, the difference between the free energy required for forming a pair of free charge carriers and that needed to form an exciton. Positive values of the exciton binding energy signify that an exciton is more stable than the free charge carriers and that additional energy needs to be invested to dissociate the exciton. This thermodynamic analysis, in the case of the exciton, can be complemented with kinetic arguments about the expected exciton lifetime based on the oscillator strength of the exciton. An alternative source of free charge carriers, beyond simple exciton dissociation described by reaction G, is as byproduct of half-reactions C and D, which can then also be thought of as describing dissociation of the exciton at the particle−water interface.

The potentials, as well as the exciton binding energy and the exciton lifetime, depend on the exact atomic geometry of the nanoparticle. As a result, the nanoparticle's properties involving free (vertical) and self-trapped (adiabatic) species are generally different. Which of these extremes is most relevant depends on the inherent time scale of the phenomena we are interested in relative to that of nuclear relaxation: much shorter, vertical, and much longer, adiabatic.

METHODS

Here we employ a combination of DFT and TD-DFT to calculate the properties of the photocatalyst nanoparticles in their different states and the potentials associated with them. We use DFT to describe the properties of the P, P^+, and P^- states and TD-DFT for those of P*. As we are modeling whole nanoparticles, we use a molecular approach, which gives us direct access to the vacuum reference state. This approach furthermore allows for convenient treatment of charged states (P^- and P^+, particle with a free electron or hole) without the need to introduce further approximations, such as a homogeneous background charge. The potentials are calculated from the DFT/TD-DFT total energies via

$$E^0 = -\frac{\Delta G(x)}{nF} \quad (1)$$

DOI: 10.1021/acs.jpcc.5b01512
J. Phys. Chem. C 2015, 119, 13384−13393

$$G(x) = U(x) + G_{vib}(x) + G_{sol}(x) \quad (2)$$

where n is the is the number of electrons involved in the half-reaction, F is the Faraday constant, U is the DFT/TD-DFT electronic total energy, G_{vib} is the sum of the vibrational, rotational, and translational contributions to the free energy, and G_{sol} is the solvation free energy.

Finally, since both of the water splitting half-reactions involve protons, for which the calculation of the free energy is a challenging task,[59,60] we use the experimentally determined absolute value of the standard hydrogen electrode (4.44 V)[61,62] for the potential of HER half-reaction. We then determine the proton free energy ($G(H^+)$), required for the calculation of the potential of the OER half-reaction, via

$$G(H^+) = \frac{1}{2}G(H_2) - \Delta G(SHE) \quad (3)$$

Within our computational scheme, we first optimize the geometry of the nanoparticle in the P, P^+, and P^- states using DFT. Second, we calculate the vertical excitation spectrum at the ground state geometry and subsequently relax the geometry of the nanoparticle in its excited P* state (modeled as the lowest singlet, S1, excitation) using TD-DFT. Third, we calculate the vertical triplet excitation energies on the P and P* geometries, as well as at an approximate T1 minimum-energy geometry obtained by optimizing the particle in its triplet state using DFT (Δ-SCF). For the solution reaction potentials, finally we optimize all relevant species using DFT and subsequently perform frequency calculations on the obtained minimum-energy structures to calculate the vibrational contribution to the free energy $G_{vib}(x)$ (see eq 2 above). For numerical tractability reasons, calculating the (excited state) frequencies of particles with more than 150 atoms is computationally very expensive, and because our experience in other systems has told us that the effect of neglecting it on the photocatalyst's potentials is generally very small,[56,57] we ignore $G_{vib}(x)$ in the case of the nanoparticle. Finally, in all calculations except when explicitly stated, the effect of bulk water is incorporated through use of a dielectric continuum solvent model, where the properties of the environment are characterized by its relative dielectric permittivity (ε). This approach allowed us to determine the contribution to the free energy of each species ($G_{sol}(x)$, see eq 2 above).

The primary nanoparticle structural model considered in this work corresponds to a solvated and hydroxylated cut of the bulk rutile structure, a 3 × 3 × 3 rutile nanoparticle previously discussed by Friesner and co-workers,[36,38,39] defined by four (110) and two (001) planes, respectively, and with a ∼1 nm core. This is perhaps the smallest rutile particle that still preserves essential features of the bulk structure. The central titanium atom in the particle has a bulklike 6-fold coordination environment, while all the other titanium atoms have at least four oxygen atoms in their first coordination sphere, of which at most two are part of a surface hydroxyl. The coordination environments of the titanium atoms at the surface of this particle are further saturated by a monolayer of molecular water. To probe methodological issues, calculations on the rutile nanoparticle were complemented with calculations on a smaller hydrated particle, $(TiO_2)_4(OH)_4(H_2O)_6$, for which some of the excited state properties were already investigated in our previous works.[53,54]

We focus in this paper on DFT and TD-DFT calculations using the CAM-B3LYP XC potential.[63] Previously, we found that use of range-separated XC potentials, such as CAM-B3LYP, was critical for a correct description of excited state properties in TiO_2 nanoparticles.[53,54] Commonly used XC potentials with no or a low percentage of Hartree−Fock like exchange (HFLE), such as PBE (0%) and B3LYP (20%), in contrast, were observed to yield generally problematic results for these particles, especially in the case of excited state relaxation, due to their inability to correctly describe so-called charge transfer (CT) states.[53,54] The latter corresponds to excitations where there is only (very) limited spatial overlap between the hole and excited electron contributions to the excited state. We complement the CAM-B3LYP calculations with selected B3LYP[64] calculations, results of which can be found in the Supporting Information.

All the DFT/TD-DFT calculations employ the all-electron double-ζ DZDP basis set (DZP for oxygen and hydrogen atoms).[65] In the CAM-B3LYP calculations, the solvent effects were approximated with the conductor-like polarizable continuum method (C-PCM)[66] dielectric solvent model, whereas for the B3LYP calculations we employed the COSMO[67] dielectric screening model. The two different approaches lead to similar results (comparisons for the B3LYP results of the test system can be found in the Supporting Information, section ESI-1), as in both cases the ε was chosen equal to 78, resembling solvation in water, and the solvation cavity for the solute was generated using van der Waals radii of 2.293, 1.72, and 1.3 Å for Ti, O, and H atoms, respectively. In all the calculations, we have considered full geometry optimizations in the presence of solvent effects except in the case of TD-DFT excitations involving the COSMO model, as no COSMO excited state gradients are currently available in the code that we use. For those B3LYP calculations, we optimized the TD-DFT excited state in vacuum and then considered the effect of COSMO as single point calculations on the gas phase excited state minimum geometries. Finally, for all the ground and excited state optimizations, the convergence criteria for the maximum Cartesian component of the gradient is chosen to be equal to 1×10^{-3} hartree $bohr^{-1}$.

All the CAM-B3LYP results were obtained using the GAMESS-US code,[68] while Turbomole[69−71] was employed for the calculations using the B3LYP XC potential. Finally, for plotting the relevant orbitals of the nanoparticles the WXMacMolPlt visualization software[72] was used.

RESULTS AND DISCUSSION

We will now discuss the predicted optical, electronic, and photocatalytic properties of the hydrated rutile nanoparticle and contrast these with those of smaller nanoparticles, as well as bulk TiO_2.

Free Exciton. The TD-CAM-B3LYP predicted optical gap of the hydrated rutile nanoparticle, the energy required to make the free S1 exciton, is 4 eV. The rutile nanoparticle is thus clearly predicted to absorb only ultraviolet or higher-energy/shorter-wavelength light, even if TD-CAM-B3LYP probably slightly overestimates the absorption onset.[53,54] The optical gap of the rutile nanoparticle is red-shifted relative to that of smaller hydroxylated nanoparticles[53,54] and blue-shifted relative to that of bulk rutile (3.0 eV).[30,34,73] While the relative size of the optical gap of the rutile nanoparticle is thus suggestive of quantum confinement, one has to be careful that one is comparing like with like (see section ESI-2 of the Supporting Information).

DOI: 10.1021/acs.jpcc.5b01512
J. Phys. Chem. C 2015, 119, 13384−13393

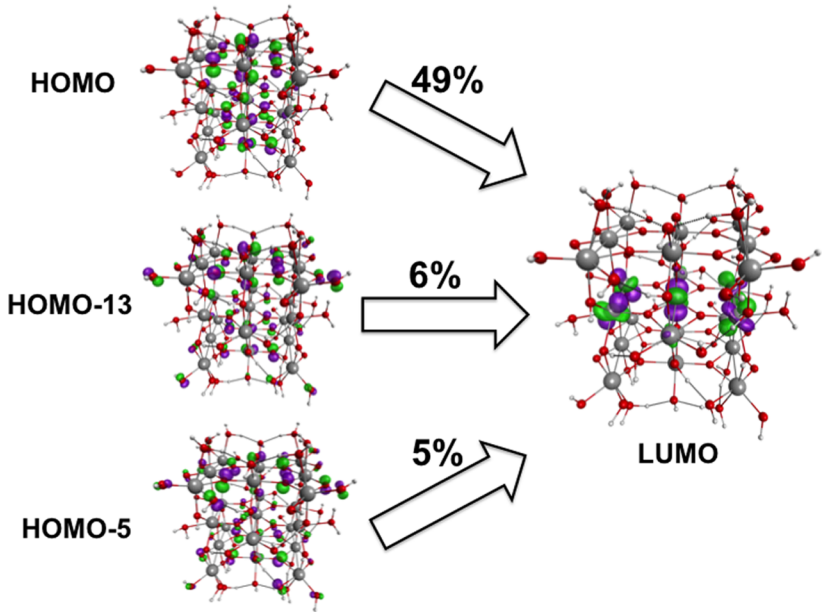

Figure 3. Leading orbital contributions to the lowest TD-CAM-B3LYP S1 excitation for the TiO_2 rutile nanoparticle (only orbitals with a contribution larger than 5% are shown). The isodensity plots for the orbitals are calculated at a value of 0.1 au, where the green and purple lobes represent the sign of the wave function (see Figure S1 in section ESI-3 of the Supporting Information for the equivalent figure for the self-trapped exciton).

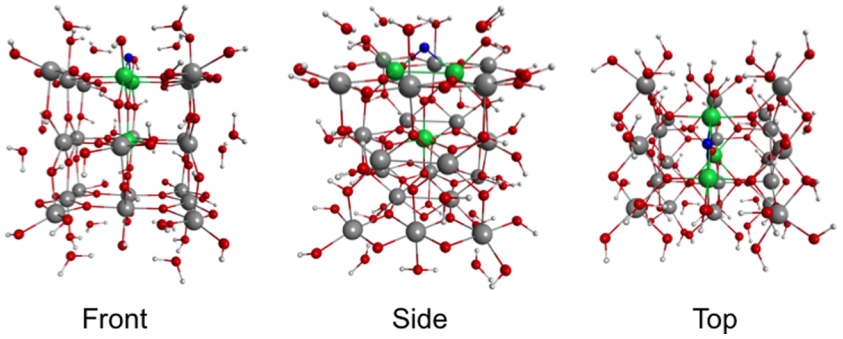

Figure 4. Geometry of the TD-CAM-B3LYP relaxed S1 excited state minimum (S1/S1min) for the TiO_2 rutile nanoparticle corresponding to the self-trapped surface exciton. Red spheres denote oxygen atoms, whereas gray and white represent titanium and hydrogen atoms, respectively. The green (Ti atoms) and blue (O atoms) spheres represent the atoms that are mostly involved with the exciton (hole and electron) self-trapping.

The excitation responsible for the S1 exciton is predicted to have essentially HOMO/VBM → LUMO/CBM character. The HOMO/VBM (hole component of the exciton) is found to essentially be delocalized over all the oxygen atoms in the core of the particle and the LUMO/CBM (excited electron component of the exciton) delocalized over the titanium atoms in the middle plane of the particle (see Figure 3). This assignment is supported by the difference between the Löwdin charges of the atoms in the ground and S1 excited state, shown in section ESI-4 of the Supporting Information. These Löwdin S1−S0 charge differences display clear evidence of excess negative charge on the titanium atoms in the middle plane (excited electron component) and excess positive charge (hole component) on the oxygen atoms in the core of the particle.

The predicted oscillator strength of the free S1 exciton is rather low (7×10^{-6}). While not dark, the absorption onset is likely to be low in intensity compared to excitonic excitations at higher energy/shorter wavelength. On the basis of this oscillator strength, the lifetime of the free S1 exciton, or at least the lifetime neglecting radiationless de-excitation through internal conversion, can be estimated using the Einstein equation to be approximately 0.2 ms, rather long in line with the low oscillator strength.

Exciton Self-Trapping. After excited state relaxation on the S1 potential energy surface, we found an excited state minimum ($S1_{min}$) at which the self-trapped S1 exciton ($S1/S1_{min}$) is 0.7 eV more stable than at the ground state geometry ($S1/S0_{min}$). The vertical singlet photoluminescence (fluorescence) signature of this self-trapped exciton is predicted to be 2.95 eV, red-shifted by ∼1.0 eV compared with the optical gap.

The considerable excited state relaxation and Stokes' shift, though smaller than that of the smaller hydrated nanoparticles previously studied,[54] are clearly linked to the significant localization induced by self-trapping. Analysis of S1−S0 Löwdin charge differences for the self-trapped exciton geometry shows that both components of the exciton have become localized on atoms on the top (110) face of the particle (see also section ESI-4 of the Supporting Information, Table S4), and we will henceforth refer to this S1 minimum as that of a self-trapped surface exciton. The majority of the hole component is localized on a two-coordinated oxygen atom and the majority of the excited electron component on two 4 + 1b + 1t

DOI: 10.1021/acs.jpcc.5b01512
J. Phys. Chem. C 2015, 119, 13384−13393

coordinated titanium atoms adjacent to this oxygen atom (see Figure 4, where 4 + 1b + 1t signifies that these titanium atoms are coordinated by four oxygen atoms, one bridging hydroxyl, and one terminal hydroxyl). The largest structural distortion associated with the exciton localization is the elongation of the bond distances between the two-coordinated oxygen atom and the two adjacent titanium atoms by ∼10%.

The oscillator strength of this S1 self-trapped surface exciton (1×10^{-6}) is slightly reduced compared to that of its free counterpart at the ground state geometry. This, together with the resulting predicted relatively long lifetime of the self-trapped exciton (3 ms), again calculated using the Einstein equation, might make the fluorescence hard to observe experimentally. Radiationless de-excitation through internal conversion, possibly coupled with phosphorescence from the lowest triplet state (T1 exciton) populated through intersystem crossing modulated by spin−orbit coupling, is likely to be the more prominent route for the system to relax back to the ground state.

The predicted bright S1 exciton lifetimes, for both the free and the self-trapped surface versions, are roughly 3 orders of magnitudes longer than the overall exciton lifetime determined experimentally for rutile single crystals through transient adsorption spectroscopy (<1 ns).[74] We cannot practically calculate the dark internal conversion contribution to the exciton de-excitation rate for such large particles. Such a calculation would require surface-hopping excited-state molecular dynamic calculations, which are currently tractable for systems containing ∼20 heavy atoms only. However, as the direct gap of bulk rutile goes together with a short exciton lifetime in rutile single crystals and vice versa the nondirect gap in bulk anatase with a long(er) exciton lifetime in anatase single crystals (>10 ns [74]), it is likely that the bulk exciton lifetime is dominated by bright de-excitation. In which case, it appears that going from the bulk to nanoparticles at least significantly reduces the bright exciton de-excitiation rate.

Excited state relaxation is also a good illustration for the need to employ the range-separated CAM-B3LYP functional when studying TiO_2 particles. As can be seen in section ESI-5 of the Supporting Information, TD-B3LYP predicts a much red-shifted fluorescence signal (1.1 eV) and a much larger energy difference between the free and self-trapped exciton ($S1/S0_{min}$ and $S1/S1_{min}$), i.e., a greater degree of excited state relaxation. Calculation of the Λ diagnostic developed by Peach et al.[75] suggests that, in line with our previous work on smaller nanoparticles,[53,54] these large differences relative to what TD-CAM-B3LYP predicts arise from the fact that the lowest singlet exciton obtains a strong charge-transfer (CT) character while relaxing. Nonhybrid XC potentials or hybrid XC potentials with a low percentage of HFLE are known to severely underestimate excitation energies of such excitations with strong CT character.[53,54] In contrast, range-separated XC-potentials, such as CAM-B3LYP, have explicitly been designed to describe both CT and local excitation in a balanced manner.

Finally, as previously observed for ZnS nanoparticles,[76,77] further self-trapped exciton minima might exist beyond the minimum corresponding to the self-trapped surface exciton discussed above, where the latter additional minima are separated on the S1 potential energy surface from the ground state geometry by an energetic barrier. Indeed S1 relaxation starting from the approximate T1 minimum energy geometry obtained through Δ-SCF (see below) rather than the ground state geometry finds a second alternative S1 self-trapped exciton minimum energy geometry. This self-trapped exciton, which is a further 0.23 eV more stable than the surface self-trapped exciton, is localized on the center of the particle rather than the surface (for more details see section ESI-6 of the Supporting Information) and will henceforth be referred to as the bulklike exciton, where the latter name makes reference to the coordination of the atoms involved rather than the properties of the exciton.

Free Electron and Hole. The rutile nanoparticle is predicted using CAM-B3LYP to have a vertical ionization potential of 7.92 eV and a vertical electron affinity of 3.44 eV. The energy required to make a pair of free charge carriers, the quasiparticle or band gap, therefore is calculated to be 4.48 eV. As a result, our calculations suggest that 0.48 eV is required to ionize the S1 exciton into a free electron on one particle and a free hole on another particle (the rutile nanoparticle is too small for an excited electron and hole to be separated sufficiently far for them to not interact). The predicted vertical EA and IP values for the rutile nanoparticle are similar in magnitude as those calculated for the low-energy (non-hydrated) bulk rutile surfaces using GW/DFT.[35] This is especially true in the case of the vertical IP potential (IP_{110} of 7.51 eV), while the vertical EA potential of the nanoparticle is more negative than its predicted bulk analogue (EA_{110} of 4.67 eV).

Just as the S1 exciton, both the excess electron and hole are predicted to strongly and barrierlessly self-trap as small polarons on fragments of the rutile nanoparticle with self-trapping energies of 1.1 and 2.2 eV, respectively. The adiabatic ionization potential therefore at 5.75 eV is significantly reduced relative to its vertical counterpart, while the adiabatic electron affinity is moderately larger than the vertical electron affinity at 4.52 eV. Calculations using the B3LYP XC potential, see section ESI-5 of the Supporting Information, predict similar behavior. More importantly perhaps, dissociation of the (surface self-trapped) exciton into a self-trapped electron on one particle and self-trapped hole on another particle is strongly favored energetically (by 2.10 eV).

On the basis of an analysis of the Löwdin spin population, the free electron self-trapping is associated with a complete localization of the excess electron on the central six-coordinated titanium atom, forming in essence a Ti^{3+} center (see Table S7 in section ESI-7 of the Supporting Information). The latter six-coordinated titanium atom is the same atom on which the excited electron component of the exciton is predicted to localize on in the case of the bulk-like self-trapped exciton. The hole in comparison is predicted to self-trap nearly completely on a two-coordinated oxygen atom on the top (110) face of particle, forming an O^- center (see Table S8 in section ESI-7 of the Supporting Information). The latter two-coordinated oxygen atom is the same atom where the hole component of the self-trapped surface exciton is predicted to localize. In both cases the trapping is associated with elongation of the bonds around the atom on which the charge becomes trapped (by 3−5% in the case of the trapped electron and 13.5−14.5% for the trapped hole).

The calculated electron self-trapping energy for the rutile nanoparticle ($3 \times 3 \times 3$) is slightly larger than predicted by Friesner and co-workers for its larger $5 \times 5 \times 5$ counterpart (0.45 eV).[38] The free charge-carrier trapping energies predicted for the rutile nanoparticle are also considerably larger than those previously reported for bulk rutile and (nonhydrated) rutile surfaces,[27−29] irrespective of the XC potential used (see

DOI: 10.1021/acs.jpcc.5b01512
J. Phys. Chem. C 2015, 119, 13384−13393

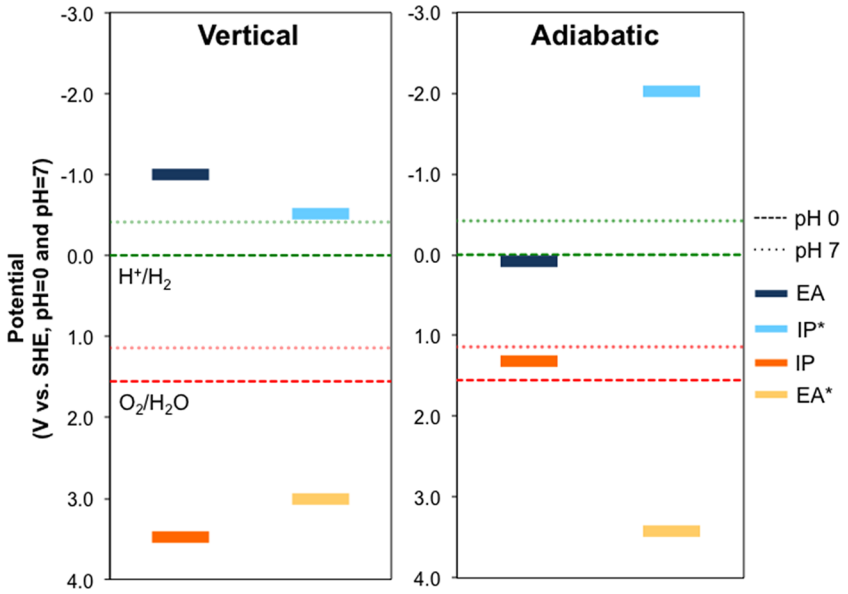

Figure 5. (TD-)CAM-B3LYP predicted EA, IP, EA*, and IP* vertical and adiabatic potentials of the TiO_2 rutile nanoparticle in water (ε = 78.0), compared to the HER (green line) and OER (red line) potentials at pH = 0 (broken lines) and pH = 7 (dotted lines). Adiabatic EA* and IP* potentials were calculated for the case of the self-trapped surface exciton; see Figure S4 in the Supporting Information for the equivalent figure for the case of the bulk-like self-trapped exciton.

also section ESI-5 of the Supporting Information), even while similar small polaron Ti^{3+}/O^{-} centers are formed in both the bulk and the nanoparticle. This is especially apparent in the case of the free hole, where the trapping energy found for the rutile nanoparticle is an order of magnitude larger than that calculated for bulk rutile[27] and more than 2 times as large as that predicted for different unhydrated rutile surfaces.[28]

Triplet Exciton. A triplet exciton (T1) can be formed from the S1 exciton through intersystem crossing, mediated by spin−orbit coupling. At the ground state geometry the free T1 exciton is effectively degenerate with the free S1 exciton (Δ_{S-T} < 5 meV). We cannot perform a TD-DFT energy minimization for the T1 exciton because the code we use for the TD-CAM-B3LYP calculations lacks analytical TD-DFT gradients for triplet excited states (see section ESI-8 of the Supporting Information for a discussion of Δ-SCF results). However, as the T1 and S1 excitons are also effectively degenerate at both the S1 surface and bulklike self-trapped exciton geometries (Δ_{S-T} < 15 meV), this singlet/triplet near degeneracy appears to be a global feature of the rutile nanoparticle S1/T1 excited-state potential energy surfaces.

Redox Potentials. Using the information discussed above, one can calculate the reduction potentials associated with the free charge carriers and the excitons. Figure 5 shows the (TD-)CAM-B3LYP predicted vertical and adiabatic potentials relative to the standard hydrogen electrode, considering the self-trapped surface exciton in the case of the adiabatic IP* and EA* potentials. Figure 5 also includes the potentials for the reduction of protons and the oxidation of water, as calculated with CAM-B3LYP. While CAM-B3LYP improves the description of excited states in TiO_2 relative to B3LYP, it gives a slightly worse description of the water potentials, overestimating the potential difference associated with the overall water splitting reaction (1.55 V CAM-B3LYP and 1.05 V B3LYP vs 1.23 V experimentally). The potentials for the water half-reaction are given both for the case of pH 0 and pH 7. The latter case is probably most relevant, not only because pH 7 is the pH of fresh water but also because we study here a rutile nanoparticle that is not (de)protonated and pH 7 is closer to the point of zero charge of rutile TiO_2 (∼pH 5) than pH 0. A plot of the potentials calculated with (TD-)B3LYP can be found in the Supporting Information (Figure S3 in section ESI-5).

The vertical and adiabatic potentials predicted by (TD-)CAM-B3LYP, in Figure 5, are rather different, something not observed for polymer photocatalysts.[56,57] Focusing first on the vertical potentials, there is a clear driving force for water oxidation by both free holes (IP) and the free exciton (EA*) in this case. There is also a small driving force for proton reduction by both the free electron (EA) and free exciton (IP*). The adiabatic potentials, however, suggest that after self-trapping both proton reduction and water oxidation by self-trapped charge carriers are endergonic, while both are strongly exergonic in the case of the self-trapped exciton. This latter is of limited practical use, however, as reduction or oxidation driven by the self-trapped exciton (IP* and EA*, half-reactions C and D) inherently generates the self-trapped free charge carriers discussed above that are chemically inert with respect to water and do not take part in any further reaction. The adiabatic exciton potentials IP* and EA* predicted for the case of the bulklike self-trapped exciton, see Figure S4 in the Supporting Information, are very similar to those in Figure 5 calculated for the self-trapped surface exciton, suggesting that the above observations are relatively insensitive to the exact localization of the self-trapped exciton.

These observations are not unique to (TD-)CAM-B3LYP; the free charge carriers potentials calculated with (TD-)B3LYP in the Supporting Information show very similar behavior (see Figure S3 in section ESI-5 of the Supporting Information; the adiabatic exciton potentials IP* and EA*, in contrast, are rather different because of the problems of TD-B3LYP to accurately describe charge-transfer excitations, discussed above). Potentials for the triplet exciton are not shown in Figures 5 and S4, but because of the observed apparent near degeneracy between

DOI: 10.1021/acs.jpcc.5b01512
J. Phys. Chem. C 2015, 119, 13384−13393

the T1 and S1 exciton, discussed above, they are expected to lie very close if not on top of their S1 equivalents.

Water Splitting and the Effect of Particle Size. The rutile nanoparticle potentials discussed above present an interesting situation, where the system's thermodynamic ability to drive the water splitting half reactions is significantly different for free and self-trapped electronic states. To a certain extent, the sets of vertical and adiabatic potentials represent two different physical limits. Vertical potentials describe the situation where the rate of the elementary half-reactions driven by the photocatalyst, or the rate of hole and/or electron transport to a cocatalyst, is significantly faster than the nuclear relaxation associated with self-trapping, while adiabatic potentials represent the exact opposite limit. In the absence of the ability to perform ab initio surface-hopping excited-state molecular dynamics calculations on such particles, it is difficult to be sure which situation is most realistic for a working rutile nanoparticulate photocatalyst. However, as the rate of any chemical surface reaction is likely to be at best comparable to the rate of nuclear relaxation in the particle, the adiabatic case is probably the most relevant in practice. This would mean that small rutile nanoparticles, like that studied here, are thermodynamically unable to drive the splitting of water.

Building forward on this analysis, one can speculate that the fact that the vertical and adiabatic potentials are significantly different might be one of the reasons behind the experimentally observed change in water splitting activity with particle size. To investigate this hypothesis, we would ideally compare the vertical and adiabatic potentials calculated for the rutile nanoparticles and the rutile bulk. While, as discussed above, calculated vertical potentials for rutile slabs with different surfaces have been reported in the literature, we are not aware of any calculated adiabatic potentials for bulk rutile (surfaces). However, as the difference between the vertical and adiabatic potentials in the case of the free charge carriers (half-reactions E and F, EA and IP) is essentially their respective self-trapping energies, we can use the self-trapping energies predicted for the nanoparticle and the bulk to estimate how the difference between the two sets of potentials might change with particle size.

As discussed above, irrespective of the XC potential used, the free charge carrier self-trapping energies predicted for the rutile nanoparticle are considerably larger than those previously reported for bulk rutile and rutile surfaces, as well as slightly larger than those calculated for a larger rutile nanoparticle. It thus stands to reason that the magnitude of the difference between the adiabatic and vertical potentials will decrease with increasing particle size and will be at its largest for small nanoparticles. Assuming that the vertical potentials are relatively independent of particle size, in line with the observed similarities between our calculated nanoparticle's vertical potentials and those reported for bulk slabs, this would suggest that the driving forces for reduction and oxidation by self-trapped free charge carriers (IP and EA) are smallest for rutile nanoparticles and will increase with increasing particle size. Following the same logic, and while we lack information on the self-trapping of excitons for bulk rutile (surfaces), it is likely that the difference between the vertical and adiabatic potentials involving the exciton (IP* and EA*) should also decrease with increasing particle size. Assuming again roughly constant vertical potentials, the driving forces for reduction and oxidation by the self-trapped exciton would then be largest for rutile nanoparticles and decrease with increasing particle size. Overall, this approximate analysis thus suggests that on thermodynamic grounds the activity of rutile nanoparticles should decrease when reducing the particle size and that the limiting factor is the decline in the driving forces for oxidation and reduction by the free charge carriers.

The origin of these large differences between the vertical and adiabatic potentials for the nanoparticle, as well as the large underlying self-trapping energies, is most likely the fact that the structure of nanoparticles is much less constrained, more polarizable, compared to that of bulk rutile TiO_2 and even bulk surfaces. The atoms in the nanoparticle are therefore freer to move when accommodating the strain associated with the localization of a free charge carrier or exciton on them, allowing for a larger degree of self-trapping.

CONCLUSIONS

We predict that small rutile TiO_2 nanoparticles are thermodynamically unable to drive photocatalytic water splitting because of the strong self-trapping of free electrons and holes in such nanoparticles. A comparison with the self-trapping energy values calculated for free charge carriers in bulk rutile (surfaces), which are much smaller, further suggests that the experimentally observed reduction in water splitting activity with particle size might be the direct result of the increased stabilization of self-trapped free charge carriers, relative to their nontrapped counterparts, in nanoparticles. The origin of the strong self-trapping of free charge carriers in small nanoparticles is probably related to the fact that the atoms on the surfaces of these nanoparticles are structurally less constrained, even relative to atoms on bulk surfaces.

ASSOCIATED CONTENT

Supporting Information

(TD-)B3LYP and (TD-)CAM-B3LYP data for the rutile nanoparticle, as well as data for smaller nanoparticles, the bulk-like self-trapped exciton minimum energy geometry, and results from Δ-SCF calculations for the lowest triplet excited state. The Supporting Information is available free of charge on the ACS Publications website at DOI: 10.1021/acs.jpcc.5b01512.

AUTHOR INFORMATION

Corresponding Author

*E-mail: m.zwijnenburg@ucl.ac.uk. Phone: +44-(0)20-7679 4665.

Notes

The authors declare no competing financial interest.

ACKNOWLEDGMENTS

We kindly acknowledge Prof. S. Bromley, Dr. C. Butchosa, Dr. A. Cowan, Prof. F. Illas, P. Guiglion, Dr. K. Kowalski, Prof. F. Osterloh, Prof. I. Parkin, Dr. S. Shevlin, Prof. A. Shluger, Prof. F. Furche, Dr. Monica Calatayud, Dr. A. A. Sokol, and Dr. S. Woodley for stimulating discussions. M.A.Z. acknowledges the UK Engineering and Physical Sciences Research Council (EPSRC) for a Career Acceleration Fellowship (Grant EP/I004424/1). This study has further been supported by a UCL Impact studentship award to E.B. Computational time on the computers of the Unity High Performance Computing Facility at University College London, the IRIDIS regional high-performance computing service provided by the e-Infrastructure South Centre for Innovation (EPSRC Grants EP/

DOI: 10.1021/acs.jpcc.5b01512
J. Phys. Chem. C 2015, 119, 13384−13393

K000144/1 and EP/K000136/1), and ARCHER the UK's national high-performance computing service (via our membership of the UK's HPC Materials Chemistry Consortium, which is funded by EPSRC grant EP/L000202/1) is gratefully acknowledged.

REFERENCES

(1) Maeda, K. Direct Splitting Of Pure Water Into Hydrogen And Oxygen Using Rutile Titania Powder As A Photocatalyst. *Chem. Commun.* **2013**, *49*, 8404−8406.
(2) Maeda, K. Photocatalytic Properties Of Rutile TiO_2 Powder For Overall Water Splitting. *Catal. Sci. Technol.* **2014**, *4*, 1949−1953.
(3) Maeda, K.; Murakami, N.; Ohno, T. Dependence of Activity of Rutile Titanium(IV) Oxide Powder for Photocatalytic Overall Water Splitting on Structural Properties. *J. Phys. Chem. C* **2014**, *118*, 9093−9100.
(4) Amano, F.; Nakata, M.; Ishinaga, E. Photocatalytic Activity of Rutile Titania for Hydrogen Evolution. *Chem. Lett.* **2014**, *43*, 509−511.
(5) Sato, S.; White, J. M. Photodecomposition Of Water Over Pt/TiO_2 Catalysts. *Chem. Phys. Lett.* **1980**, *72*, 83−86.
(6) Tang, J.; Durrant, J. R.; Klug, D. R. Mechanism Of Photocatalytic Water Splitting In TiO_2. Reaction Of Water With Photoholes, Importance Of Charge Carrier Dynamics, And Evidence For Four-Hole Chemistry. *J. Am. Chem. Soc.* **2008**, *130*, 13885−13891.
(7) Banno, H.; Kariya, B.; Isu, N.; Ogawa, M.; Miwa, S.; Sawada, K.; Tsuge, J.; Imaizumi, S.; Kato, H.; Tokutake, K.; Deguchi, S. Effect of TiO_2 Crystallite Diameter on Photocatalytic Water Splitting Rate. *Green Sustainable Chem.* **2014**, *4*, 87−94.
(8) Ohno, T.; Sarukawa, K.; Matsumura, M. Photocatalytic Activities Of Pure Rutile Particles Isolated From TiO_2 Powder By Dissolving The Anatase Component In HF Solution. *J. Phys. Chem. B* **2001**, *105*, 2417−2420.
(9) Shkrob, I. A.; Sauer, M. C. Hole Scavenging And Photo-Stimulated Recombination Of Electron−Hole Pairs In Aqueous TiO_2 Nanoparticles. *J. Phys. Chem. B* **2004**, *108*, 12497−12511.
(10) Testino, A.; Bellobono, I. R.; Buscaglia, V.; Canevali, C.; D'Arienzo, M.; Polizzi, S.; Scotti, R.; Morazzoni, F. Optimizing The Photocatalytic Properties Of Hydrothermal TiO_2 By The Control Of Phase Composition And Particle Morphology. A Systematic Approach. *J. Am. Chem. Soc.* **2007**, *129*, 3564−3575.
(11) Kim, W.; Tachikawa, T.; Moon, G.-h.; Majima, T.; Choi, W. Molecular-Level Understanding Of The Photocatalytic Activity Difference Between Anatase And Rutile Nanoparticles. *Angew. Chem., Int. Ed.* **2014**, *53*, 14036−14041.
(12) Ni, M.; Leung, M. K. H.; Leung, D. Y. C.; Sumathy, K. A Review And Recent Developments In Photocatalytic Water-Splitting Using TiO_2 For Hydrogen Production. *Renewable Sustainable Energy Rev.* **2007**, *11*, 401−425.
(13) Prieto-Mahaney, O.-O.; Murakami, N.; Abe, R.; Ohtani, B. Correlation between Photocatalytic Activities and Structural and Physical Properties of Titanium(IV) Oxide Powders. *Chem. Lett.* **2009**, *38*, 238−239.
(14) Abe, R. Development Of A New System For Photocatalytic Water Splitting Into H_2 And O_2 Under Visible Light Irradiation. *Bull. Chem. Soc. Jpn.* **2011**, *84*, 1000−1030.
(15) Ravelli, D.; Dondi, D.; Fagnoni, M.; Albini, A. Photocatalysis. A Multi-Faceted Concept For Green Chemistry. *Chem. Soc. Rev.* **2009**, *38*, 1999−2011.
(16) Li, G.; Gray, K. A. The Solid−Solid Interface: Explaining The High And Unique Photocatalytic Reactivity Of TiO_2-Based Nanocomposite Materials. *Chem. Phys.* **2007**, *339*, 173−187.
(17) Kumar, S. G.; Devi, L. G. Review on Modified TiO_2 Photocatalysis under UV/Visible Light: Selected Results and Related Mechanisms on Interfacial Charge Carrier Transfer Dynamics. *J. Phys. Chem. A* **2011**, *115*, 13211−13241.
(18) Scanlon, D. O.; Dunnill, C. W.; Buckeridge, J.; Shevlin, S. A.; Logsdail, A. J.; Woodley, S. M.; Catlow, C. R. A.; Powell, M. J.; Palgrave, R. G.; Parkin, I. P.; Watson, G. W.; Keal, T. W.; Sherwood, P.; Walsh, A.; Sokol, A. A. Band Alignment Of Rutile And Anatase TiO_2. *Nat. Mater.* **2013**, *12*, 798−801.
(19) Kapilashrami, M.; Zhang, Y.; Liu, Y.-S.; Hagfeldt, A.; Guo, J. Probing the Optical Property and Electronic Structure of TiO_2 Nanomaterials for Renewable Energy Applications. *Chem. Rev.* **2014**, *114*, 9662−9707.
(20) Quesada-Cabrera, R.; Sotelo-Vazquez, C.; Bear, J. C.; Darr, J. A.; Parkin, I. P. Photocatalytic Evidence of the Rutile-to-Anatase Electron Transfer in Titania. *Adv. Mater. Interfaces* **2014**, *1*, 1−7.
(21) Ohtani, B.; Ogawa, Y.; Nishimoto, S. Photocatalytic Activity Of Amorphous-Anatase Mixture Of Titanium(IV) Oxide Particles Suspended In Aqueous Solutions. *J. Phys. Chem. B* **1997**, *101*, 3746−3752.
(22) Kočí, K.; Obalová, L.; Matějová, L.; Plachá, D.; Lacný, Z.; Jirkovský, J.; Šolcová, O. Effect Of TiO_2 Particle Size On The Photocatalytic Reduction Of CO_2. *Appl. Catal., B* **2009**, *89*, 494−502.
(23) Anpo, M.; Shima, T.; Kodama, S.; Kubokawa, Y. Photocatalytic Hydrogenation Of Propyne With Water On Small-Particle Titania: Size Quantization Effects And Reaction Intermediates. *J. Phys. Chem.* **1987**, *91*, 4305−4310.
(24) Xu, N. P.; Shi, Z. F.; Fan, Y. Q.; Dong, J. H.; Shi, J.; Hu, M. Z. C. Effects Of Particle Size Of TiO_2 On Photocatalytic Degradation Of Methylene Blue In Aqueous Suspensions. *Ind. Eng. Chem. Res.* **1999**, *38*, 373−379.
(25) Mattioli, G.; Alippi, P.; Filippone, F.; Caminiti, R.; Amore Bonapasta, A. Deep versus Shallow Behavior of Intrinsic Defects in Rutile and Anatase TiO_2 Polymorphs. *J. Phys. Chem. C* **2010**, *114*, 21694−21704.
(26) Di Valentin, C.; Selloni, A. Bulk and Surface Polarons in Photoexcited Anatase TiO_2. *J. Phys. Chem. Lett.* **2011**, *2*, 2223−2228.
(27) Varley, J. B.; Janotti, A.; Franchini, C.; Van de Walle, C. G. Role Of Self-Trapping In Luminescence And p-Type Conductivity Of Wide-Band-Gap Oxides. *Phys. Rev. B* **2012**, *85*, 0811091−0811094.
(28) Zawadzki, P.; Laursen, A. B.; Jacobsen, K. W.; Dahl, S.; Rossmeisl, J. Oxidative Trends Of TiO_2-Hole Trapping At Anatase And Rutile Surfaces. *Energy Environ. Sci.* **2012**, *5*, 9866−9869.
(29) Spreafico, C.; VandeVondele, J. The Nature Of Excess Electrons In Anatase And Rutile From Hybrid DFT And RPA. *Phys. Chem. Chem. Phys.* **2014**, *16*, 26144−26152.
(30) Dehaart, L. G. J.; Blasse, G. The Observation Of Exciton Emission From Rutile Single-Crystals. *J. Sol. State Chem.* **1986**, *61*, 135−136.
(31) Sildos, I.; Suisalu, A.; Aarik, J.; Sekiya, T.; Kurita, S. Self-Trapped Exciton Emission In Crystalline Anatase. *J. Lumin.* **2000**, *87*−*89*, 290−292.
(32) Watanabe, M.; Hayashi, T. Time-Resolved Study Of Self-Trapped Exciton Luminescence In Anatase TiO_2 Under Two-Photon Excitation. *J. Lumin.* **2005**, *112*, 88−91.
(33) Kernazhitsky, L.; Shymanovska, V.; Gavrilko, T.; Naumov, V.; Fedorenko, L.; Kshnyakin, V.; Baran, J. Room Temperature Photoluminescence Of Anatase And Rutile TiO_2 Powders. *J. Lumin.* **2014**, *146*, 199−204.
(34) Pascual, J.; Camassel, J.; Mathieu, H. Fine Structure In The Intrinsic Absorption Edge Of TiO_2. *Phys. Rev. B* **1978**, *18*, 5606−5614.
(35) Stevanovic, V.; Lany, S.; Ginley, D. S.; Tumas, W.; Zunger, A. Assessing Capability Of Semiconductors To Split Water Using Ionization Potentials And Electron Affinities Only. *Phys. Chem. Chem. Phys.* **2014**, *16*, 3706−3714.
(36) Blagojevic, V.; Chen, Y.-R.; Steigerwald, M.; Brus, L.; Friesner, R. A. Quantum Chemical Investigation of Cluster Models for TiO_2 Nanoparticles with Water-Derived Ligand Passivation: Studies of Excess Electron States and Implications for Charge Transport in the Gratzel Cell. *J. Phys. Chem. C* **2009**, *113*, 19806−19811.
(37) Li, Y.-F.; Liu, Z.-P. Particle Size, Shape And Activity For Photocatalysis On Titania Anatase Nanoparticles In Aqueous Surroundings. *J. Am. Chem. Soc.* **2011**, *133*, 15743−15752.
(38) Zhang, J.; Hughes, T. F.; Steigerwald, M.; Brus, L.; Friesner, R. A. Realistic Cluster Modeling of Electron Transport and Trapping in

DOI: 10.1021/acs.jpcc.5b01512
J. Phys. Chem. C 2015, 119, 13384−13393

Solvated TiO_2 Nanoparticles. *J. Am. Chem. Soc.* **2012**, *134*, 12028−12042.
(39) Zhang, J.; Steigerwald, M.; Brus, L.; Friesner, R. A. Covalent O-H Bonds as Electron Traps in Proton-Rich Rutile TiO_2 Nanoparticles. *Nano Lett.* **2014**, *14*, 1785−1789.
(40) Rocca, D.; Gebauer, R.; De Angelis, F.; Nazeeruddin, M. K.; Baroni, S. Time-Dependent Density Functional Theory Study Of Squaraine Dye-Sensitized Solar Cells. *Chem. Phys. Lett.* **2009**, *475*, 49−53.
(41) Shevlin, S. A.; Woodley, S. M. Electronic and Optical Properties of Doped and Undoped $(TiO_2)_n$ Nanoparticles. *J. Phys. Chem. C* **2010**, *114*, 17333−17343.
(42) Taylor, D. J.; Paterson, M. J. Calculations Of The Low-Lying Excited States Of The TiO_2 Molecule. *J. Chem. Phys.* **2010**, *133*, 204302.
(43) Sanchez-de-Armas, R.; Oviedo, J.; San-Miguel, M. A.; Sanz, J. F. Real-time TD-DFT Simulations in Dye Sensitized Solar Cells: The Electronic Absorption Spectrum of Alizarin Supported on TiO_2 Nanoclusters. *J. Chem. Theory Comput.* **2010**, *6*, 2856−2865.
(44) De Angelis, F.; Fantacci, S.; Gebauer, R. Simulating Dye-Sensitized TiO_2 Heterointerfaces in Explicit Solvent: Absorption Spectra, Energy Levels, and Dye Desorption. *J. Phys. Chem. Lett.* **2011**, *2*, 813−817.
(45) Chiodo, L.; Salazar, M.; Romero, A. H.; Laricchia, S.; Della Sala, F.; Rubio, A. Structure, Electronic, And Optical Properties Of TiO_2 Atomic Clusters: An Ab Initio Study. *J. Chem. Phys.* **2011**, *135*, 244704.
(46) Auvinen, S.; Alatalo, M.; Haario, H.; Jalava, J. P.; Lamminmäki, R. J. Size And Shape Dependence Of The Electronic And Spectral Properties In TiO_2 Nanoparticles. *J. Phys. Chem. C* **2011**, *115*, 8484−8493.
(47) Taylor, D. J.; Paterson, M. J. Vibronic Coupling Effects On The Structure And Spectroscopy Of Neutral And Charged TiO_2 Clusters. *Chem. Phys.* **2012**, *408*, 1−10.
(48) Berardo, E.; Hu, H.; Kowalski, K.; Zwijnenburg, A. M. Coupled Cluster Calculations On TiO_2 Nanoclusters. *J. Chem. Phys.* **2013**, *139*, 0643131.
(49) Galynska, M.; Persson, P. Emerging Polymorphism in Nanostructured TiO_2: Quantum Chemical Comparison of Anatase, Rutile, and Brookite Clusters. *Int. J. Quantum Chem.* **2013**, *113*, 2611−2620.
(50) Kandada, A. R.; Fantacci, S.; Guarnera, S.; Polli, D.; Lanzani, G.; De Angelis, F.; Petrozza, A. Role Of Hot Singlet Excited States In Charge Generation At The Black Dye/TiO_2 Interface. *ACS Appl. Mater. Interfaces* **2013**, *5*, 4334−4339.
(51) Mattioli, G.; Amore Bonapasta, A.; Bovi, D.; Giannozzi, P. Photocatalytic and Photovoltaic Properties of TiO_2 Nanoparticles Investigated by Ab Initio Simulations. *J. Phys. Chem. C* **2014**, *118*, 29928−29942.
(52) Hung, L.; Baishya, K.; Öğüt, S. First-Principles Real-Space Study Of Electronic And Optical Excitations In Rutile. *Phys. Rev. B* **2014**, *90*, 165424.
(53) Berardo, E.; Hu, H.-S.; Shevlin, S. A.; Woodley, S. M.; Kowalski, K.; Zwijnenburg, M. A. Modeling Excited States in TiO_2 Nanoparticles: On the Accuracy of a TD-DFT Based Description. *J. Chem. Theory Comput.* **2014**, *10*, 1189−1199.
(54) Berardo, E.; Hu, H.-S.; van Dam, H. J. J.; Shevlin, S. A.; Woodley, S. M.; Kowalski, K.; Zwijnenburg, M. A. Describing Excited State Relaxation and Localization in TiO_2 Nanoparticles Using TD-DFT. *J. Chem. Theory Comput.* **2014**, *10*, 5538−5548.
(55) Nunzi, F.; Agrawal, S.; Selloni, A.; De Angelis, F. Structural and Electronic Properties of Photoexcited TiO_2 Nanoparticles from First Principles. *J. Chem. Theory Comput.* **2015**, *11*, 635−645.
(56) Butchosa, C.; Guiglion, P.; Zwijnenburg, M. A. Carbon Nitride Photocatalysts for Water Splitting: A Computational Perspective. *J. Phys. Chem. C* **2014**, *118*, 24833−24842.
(57) Guiglion, P.; Butchosa, C.; Zwijnenburg, M. A. Polymeric Watersplitting Photocatalysts; A Computational Perspective On The Water Oxidation Conundrum. *J. Mater. Chem. A* **2014**, *2*, 11996−12004.
(58) Sprick, R. S.; Jiang, J.-X.; Bonillo, B.; Ren, S.; Ratvijitvech, T.; Guiglion, P.; Zwijnenburg, M. A.; Adams, D. J.; Cooper, A. I. Tunable Organic Photocatalysts for Visible Light-Driven Hydrogen Evolution. *J. Am. Chem. Soc.* **2015**, *137*, 3265−3270.
(59) Zhan, C.-G.; Dixon, D. A. Absolute Hydration Free Energy of the Proton from First-Principles Electronic Structure Calculations. *J. Phys. Chem. A* **2001**, *105*, 11534−11540.
(60) Bryantsev, V. S.; Diallo, M. S.; Goddard Iii, W. A. Calculation of Solvation Free Energies of Charged Solutes Using Mixed Cluster/Continuum Models. *J. Phys. Chem. B* **2008**, *112*, 9709−9719.
(61) Trasatti, S. The Concept Of Absolute Electrode Potential An Attempt At A Calculation. *J. Electroanal. Chem. Interfacial Electrochem.* **1974**, *52*, 313−329.
(62) Trasatti, S. The Absolute Electrode Potential: An Explanatory Note (Recommendations 1986). *Pure Appl. Chem.* **1986**, *58*, 955−966.
(63) Yanai, T.; Tew, D. P.; Handy, N. C. A New Hybrid Exchange-Correlation Functional Using The Coulomb-Attenuating Method (CAM-B3LYP). *Chem. Phys. Lett.* **2004**, *393*, 51−57.
(64) Becke, A. D. Density-Functional Thermochemistry. 3. The Role Of Exact Exchange. *J. Chem. Phys.* **1993**, *98*, 5648−5652.
(65) Godbout, N.; Salahub, D. R.; Andzelm, J.; Wimmer, E. Optimization Of Gaussian-Type Basis-Sets For Local Spin-Density Functional Calculations. 1. Boron Through Neon, Optimization Technique And Validation. *Can. J. Chem.* **1992**, *70*, 560−571.
(66) Tomasi, J.; Mennucci, B.; Cammi, R. Quantum Mechanical Continuum Solvation Models. *Chem. Rev.* **2005**, *105*, 2999−3094.
(67) Klamt, A.; Schuurmann, G. Cosmo: A New Approach To Dielectric Screening In Solvents With Explicit Expressions For The Screening Energy And Its Gradient. *J. Chem. Soc., Perkin Trans. 2* **1993**, 799−805.
(68) Schmidt, M. W.; Baldridge, K. K.; Boatz, J. A.; Elbert, S. T.; Gordon, M. S.; Jensen, J. H.; Koseki, S.; Matsunaga, N.; Nguyen, K. A.; Su, S. J.; Windus, T. L.; Dupuis, M.; Montgomery, J. A. General Atomic And Molecular Electronic-Structure System. *J. Comput. Chem.* **1993**, *14*, 1347−1363.
(69) van Wuellen, C. Shared-Memory Parallelization of the TURBOMOLE Programs AOFORCE, ESCF, and EGRAD: How to Quickly Parallelize Legacy Code. *J. Comput. Chem.* **2011**, *32*, 1195−1201.
(70) Furche, F.; Ahlrichs, R.; Haettig, C.; Klopper, W.; Sierka, M.; Weigend, F. Turbomole. *WIREs Comput. Mol. Sci.* **2014**, *4*, 91−100.
(71) Furche, F.; Ahlrichs, R. Time-Dependent Density Functional Methods For Excited State Properties. *J. Chem. Phys.* **2004**, *121*, 12772−12773.
(72) Bode, B. M.; Gordon, M. S. Macmolplt: A Graphical User Interface For Gamess. *J. Mol. Graphics Modell.* **1998**, *16*, 133−138.
(73) Amtout, A.; Leonelli, R. Optical Properties Of Rutile Near Its Fundamental Band Gap. *Phys. Rev. B* **1995**, *51*, 6842−6851.
(74) Xu, M.; Gao, Y.; Moreno, E.; Kunst, M.; Muhler, M.; Wang, Y.; Idriss, H.; Wöll, C. Photocatalytic Activity of Bulk TiO_2 Anatase and Rutile Single Crystals Using Infrared Absorption Spectroscopy. *Phys. Rev. Lett.* **2011**, *106*, 138302.
(75) Peach, M. J. G.; Benfield, P.; Helgaker, T.; Tozer, D. J. Excitation Energies In Density Functional Theory: An Evaluation And A Diagnostic Test. *J. Chem. Phys.* **2008**, *128*, 44118.
(76) Zwijnenburg, M. A. Photoluminescence In Semiconductor Nanoparticles: An Atomistic View Of Excited State Relaxation In Nanosized ZnS. *Nanoscale* **2012**, *4*, 3711−3717.
(77) Zwijnenburg, M. A. Excited State Localisation Cascades In Inorganic Semiconductor Nanoparticles. *Phys. Chem. Chem. Phys.* **2013**, *15*, 11119−11127.

DOI: 10.1021/acs.jpcc.5b01512
J. Phys. Chem. C 2015, 119, 13384−13393